1994

Spin diffusion in the one-dimensional $s = 1/2$ *XXZ* model at infinite temperature

Markus Böhm

V. S. Viswanath
University of Rhode Island

See next page for additional authors

Citation/Publisher Attribution

Markus Böhm, V.S. Viswanath, Joachim Stolze and Gerhard Müller. *Spin diffusion in the 1D s=1/2 XXZ model at infinite temperature.* Phys. Rev. B **49** (1994), 15669-15681.
Available at http://journals.aps.org/prb/abstract/10.1103/PhysRevB.49.15669.

Authors
Markus Böhm, V. S. Viswanath, Joachim Stolze, and Gerhard Müller

Spin diffusion in the one-dimensional $s=\frac{1}{2}$ XXZ model at infinite temperature

Markus Böhm
Institut für Theoretische Physik, Universität Erlangen-Nürnberg, D-91058 Erlangen, Germany

V. S. Viswanath, Joachim Stolze,* and Gerhard Müller
Department of Physics, The University of Rhode Island, Kingston, Rhode Island 02881-0817
(Received 26 April 1993)

Time-dependent spin-autocorrelation functions at $T=\infty$ and (in particular) their spectral densities for the bulk spin and the boundary spin of the semi-infinite spin-$\frac{1}{2}$ XXZ model (with exchange parameters $J_x=J_y\equiv J, J_z$) are investigated on the basis of (i) rigorous bounds in the time domain and (ii) a continued-fraction analysis in the frequency domain. We have found strong numerical evidence for spin diffusion in quantum spin models. For J_z/J increasing from zero, the results of the short-time expansion indicate a change of the bulk-spin xx-autocorrelation function from Gaussian decay to exponential decay. The continued-fraction analysis of the same dynamic quantity signals a change from exponential decay to power-law decay as J_z/J approaches unity and back to a more rapid decay upon further increase of that parameter. By contrast, the change in symmetry at $J_z/J=1$ has virtually no impact on the bulk-spin zz-autocorrelation function (as expected). Similar contrasting properties are observable in the boundary-spin autocorrelation functions.

I. INTRODUCTION

After more than two decades of theoretical studies devoted to high-temperature dynamics of quantum spin chains, which have produced a number of intriguing exact results, one central question has remained unanswered: Does the phenomenological concept of spin diffusion provide at all an adequate description for the transport of the fluctuations of a conserved magnetization component? While the spin-diffusion phenomenon was frequently invoked for the interpretation of experimental results from inelastic neutron scattering, electron spin resonance and NMR on quasi-one-dimensional (1D) magnetic compounds,[1,2] its support by microscopic theories or numerical analysis of quantum spin dynamics has remained rather weak and tentative[3–5] or artificially imposed.[6]

Even for *classical* spin chains, whose long-time dynamics is more readily accessible to numerical analysis by means of simulation studies, the answer to that question has proven to involve unanticipated subtleties. The anomalous character of spin diffusion in the classical Heisenberg chain, identified some five years ago,[7] has remained a matter of controversy ever since as to its correct interpretation.[8–13] There is now strong evidence that the diffusivity is singular, giving rise to logarithmic corrections in the long-time tail of the spin-autocorrelation function,[12] but the exact nature of these corrections and their origin have remained obscure.

It is much more challenging to analyze the long-time dynamics of *quantum* spin chains. There are only very few quantum spin models with nontrivial dynamics for which dynamic correlation functions at $T=\infty$ have been determined exactly. Among them are the equivalent-neighbor XXZ model[14,15] and the 1D $s=\frac{1}{2}$ XY model.[16–23] Spin diffusion has no part in either model for reasons that are well understood.

For other quantum spin models with nontrivial dynamics, such as the 1D XXZ model, exact information on dynamic correlation functions is limited to a number of frequency moments obtained from $T=\infty$ expectation values of spin products.[5,24–26] The information contained in these frequency moments can be employed in two different ways to infer characteristic properties of dynamic correlation functions:

(i) We may use the frequency moments as Taylor coefficients in the short-time expansion of a correlation function. For certain situations, the rigorous upper and lower bounds thus determined for that function may yield accurate results over time intervals that are sufficiently long to unlock valuable information on the underlying physical process—information that is otherwise inaccessible.

(ii) For certain other situations, further information on the long-time behavior can be extracted from the frequency moments if they are converted into an equal number of continued-fraction coefficients for the relaxation function (the Laplace transform of the correlation function).

This paper builds principally on the accomplishments of two previous studies of $T=\infty$ quantum spin dynamics[23,25] with focus on methods (i) and (ii), respectively. Here the analytic and numerical techniques developed in those studies are combined for the specific purpose of elucidating the $T=\infty$ dynamics of the 1D $s=\frac{1}{2}$ XXZ model. The Hamiltonian for a semi-infinite chain reads

$$H_{XXZ}=-\sum_{l=0}^{\infty}\{J(S_l^xS_{l+1}^x+S_l^yS_{l+1}^y)+J_zS_l^zS_{l+1}^z\} . \quad (1.1)$$

We focus on (normalized) spin-autocorrelation functions

$$C_l^{\mu\mu}(t)\equiv\frac{\langle S_l^\mu(t)S_l^\mu\rangle}{\langle S_l^\mu S_l^\mu\rangle},\quad \mu=x,z \quad (1.2)$$

0163-1829/94/49(22)/15669(13)/$06.00

at $T=\infty$ and the associated spectral densities

$$\Phi_l^{\mu\mu}(\omega)\equiv\int_{-\infty}^{+\infty}dt\, e^{i\omega t}C_l^{\mu\mu}(t),\quad \mu=x,z\ . \tag{1.3}$$

Results will be presented for $l=\infty$ (bulk spin) and $l=0$ (boundary spin). For two special cases, the dynamics can be analyzed exactly: the XX model ($J_z=0$) is equivalent to a system of noninteracting lattice fermions, and the X model ($J=0$) is as trivial as the quantum harmonic oscillator. For other parameter values, however, the $T=\infty$ dynamics of the XXZ model is quite complicated, and transitions between different types of dynamical behavior can be studied. For that purpose, the two above-mentioned methods (i) and (ii) of analyzing frequency moments turn out to be invaluable instruments for analysis and interpretation. Our main point of emphasis is the identification of diffusive long-time tails in spin-autocorrelation functions under the right symmetry conditions or the corresponding infrared divergences in the associated spectral densities.

The phenomenon of spin diffusion is based on a thermalization process that is subject to a conservation law. The phenomenological theory in its simplest form states that the fluctuations $S^\mu(q,t)$ of any conserved spin component satisfy the diffusion equation for sufficiently long times and wavelengths. It predicts exponential decay for correlation functions that are not constrained by that conservation law and diffusive long-time tails for those that are. The fact is that exponential decay in time or diffusive long-time tails do not occur in any of the known exact results for interacting quantum spin systems. The decay in those systems turns out to be either Gaussian or nondiffusive power law. In this study we provide evidence in support of spin diffusion in the 1D $s=\frac{1}{2}$ XXZ model in the form of a crossover from Gaussian to exponential decay (Sec. III) and in the form of long-time tails that come and go with the conservation law required for diffusive behavior (Secs. IV–VI). The presentation of the results is preceded (Sec. II) by a brief description of the two main methods of analysis employed here.

II. CALCULATIONAL TECHNIQUES

At $T=\infty$, the spin-autocorrelation function (1.2) is real and symmetric. It can be expanded into a power series of the form

$$C_l^{\mu\mu}(t)=\sum_{k=0}^{\infty}\frac{(-1)^k}{(2k)!}M_{2k}^{\mu\mu}(l)t^{2k}\ , \tag{2.1}$$

where the expansion coefficients are the frequency moments of the spectral density (1.3)

$$M_{2k}^{\mu\mu}(l)=\int_{-\infty}^{+\infty}\frac{d\omega}{2\pi}\omega^{2k}\Phi_l^{\mu\mu}(\omega)$$
$$=(-1)^k\left[\frac{d^{2k}}{dt^{2k}}C_l^{\mu\mu}(t)\right]_{t=0},\quad k=0,1,2,\ldots, \tag{2.2}$$

and can be expressed as expectation values

$$M_{2k}^{\mu\mu}(l)=-(-1)^l\langle[\cdots[S_l^\mu,H],\ldots,H][\cdots[S_l^\mu,H],\ldots,H]\rangle/\langle S_l^\mu S_l^\mu\rangle \tag{2.3}$$

of operators produced by the product of two k-fold commutators.[5,25] These expectation values can be evaluated exactly by readily programmable integer arithmetic as explained in Ref. 25. We have determined the $M_{2k}^{\mu\mu}(l)$ up to $k=14$ for the bulk spin ($l=\infty$) of the XXZ model and up to $k=17$ for the boundary spin ($l=0$). This represents a significant advance from previously known moments for that model.[5,24] The exact moments are listed in Appendix A.

In Sec. III we shall use these expansion coefficients to determine upper and lower bounds of the spin-autocorrelation function by methods that have been developed and described previously.[5,24–27] In Secs. IV–VI the information contained in the frequency moments will be analyzed by quite different methods. We convert the $M_{2k}^{\mu\mu}(l)$ into the continued-fraction coefficients $\Delta_k^{\mu\mu}(l)$ of the relaxation function

$$c_l^{\mu\mu}(z)\equiv\int_0^\infty dt\, e^{-zt}C_l^{\mu\mu}(t)=\cfrac{1}{z+\cfrac{\Delta_1^{\mu\mu}(l)}{z+\cfrac{\Delta_2^{\mu\mu}(l)}{z+\cdots}}}, \tag{2.4}$$

which is the Laplace transform of the spin-autocorrelation function (1.2), and proceed with the analysis from there. A set of transformation formulas between the first K frequency moments $M_{2k}^{\mu\mu}(l)$ and the first K coefficients $\Delta_k^{\mu\mu}(l)$ is given in Appendix B.

It must be mentioned that the continued-fraction coefficients $\Delta_k^{\mu\mu}(l)$ can be determined more directly by means of the recursion method. The computational effort is almost identical to that required for the determination of an equal number of frequency moments $M_{2k}^{\mu\mu}(l)$. A brief account of Lee's[28] formulation of the recursion method as applied to quantum spin dynamics at high temperature was given in Refs. 15, 21, and 23 for several applications.

In this paper, the known continued-fraction coefficients $\Delta_k^{\mu\mu}(l)$ will be analyzed along two different lines: (a) We shall reconstruct the spectral density (1.3) from the relaxation function (2.4) via the relation

$$\Phi_l^{\mu\mu}(\omega)=2\lim_{\varepsilon\to 0}\mathcal{R}[c_l^{\mu\mu}(\varepsilon-i\omega)] \tag{2.5}$$

by methods involving the use of matching termination functions that have previously been tested and applied in quantum spin dynamics.[23,29,30] (b) We shall employ the method developed in Ref. 30 for the identification of infrared singularities in spectral densities by direct analysis of the known sequence of $\Delta_k^{\mu\mu}(l)$.

III. FROM GAUSSIAN DECAY TO EXPONENTIAL RELAXATION

Consider first the bulk-spin autocorrelation function $\langle S_\infty^x(t)S_\infty^x\rangle$ of the *XXZ* model (1.1). The nontrivial but exactly solvable case $J_z=0$ (*XX* model) is an ideal starting point for the analysis of the *XXZ* cases by both calculational techniques we intend to employ. The well-known exact expressions for that autocorrelation function and its spectral density in the *XX* limit read:[18–21]

$$\langle S_\infty^x(t)S_\infty^x\rangle=\langle S_\infty^y(t)S_\infty^y\rangle=\tfrac{1}{4}e^{-J^2t^2/4}\ , \tag{3.1}$$

$$\Phi_\infty^{xx}(\omega)=\frac{2\sqrt{\pi}}{J}e^{-\omega^2/J^2}\ . \tag{3.2}$$

The Gaussian decay of (3.1) is clearly anomalous, attributable to the free-fermion nature of the *XX* model. The default expectation within the spin-diffusion scenario would be exponential decay at long times instead. The nongeneric processes that govern the transport of spin fluctuations in the *XX* model are further indicated by the fact that all pair-correlation functions $\langle S_l^x(t)S_{l'}^x\rangle$, $l\neq l'$ are identically zero. In the *XXZ* model, the anomalous features are expected to disappear. A weak fermion interaction (with coupling constant J_z) impacts the long-time behavior more strongly than it affects the short-time behavior. In the function $\langle S_\infty^x(t)S_\infty^x\rangle$ we thus expect to see a crossover from a Gaussian behavior at short times to exponential decay at longer times. The very simple structure of the exact result (3.1) makes it possible to observe clear indicators for such a crossover in a short-time expansion at $J_z\ll J$.

In Fig. 1 we have plotted the function $\ln(\langle S_\infty^x(t)S_\infty^x\rangle)/(Jt\langle S_\infty^xS_\infty^x\rangle)$ versus Jt for four different parameter values of the *XXZ* model near the *XX* limit. The straight dashed line with negative slope represents the pure Gaussian (3.1). The results for $J_z\neq0$ show strong indications that the decay is slower than Gaussian, consistent with exponential decay (convergence toward a negative constant in the plot of Fig. 1). Power-law decay would imply convergence toward zero. Whether or not the observed exponential decay represents the true asymptotic behavior is, of course, beyond the reach of this type of analysis.

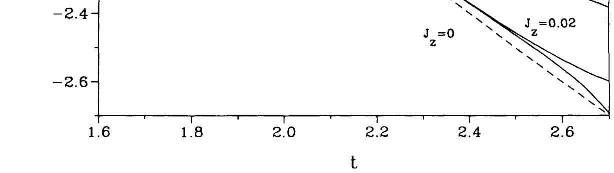

FIG. 1. Short-time expansion of the spin-autocorrelation function $C_\infty^{xx}(t)=\langle S_\infty^x(t)S_\infty^x\rangle/\langle S_\infty^xS_\infty^x\rangle$ at $T=\infty$ of the 1D $s=\frac{1}{2}$ *XXZ* model for $J=1$ and $J_z=0.02$, 0.05, 0.1 (solid lines) near the exactly solvable case $J_z=0$ (dashed line). The data are plotted in a way suitable for visualizing the crossover from Gaussian decay (negative unit slope) to exponential decay (zero slope). Each result of the short-time expansion is represented by two curves corresponding to an upper and a lower bound of the function. The bounds have been determined from 14 exact frequency moments $M_{2k}^{xx}(\infty)$.

IV. FROM EXPONENTIAL RELAXATION TO DIFFUSIVE LONG-TIME TAILS

Unlike in classical spin dynamics, where diffusive long-time tails are readily detectable in simulation data and directly amenable to a quantitative analysis, the most direct indicators of their presence in quantum spin dynamics (at least in 1D and 2D systems) are infrared divergences in spectral densities. The continued-fraction analysis is an ideal instrument for the quantitative study of such singularities.

A. Δ_k sequences and model spectral densities

The exact result (3.2) for the spectral density $\Phi_\infty^{xx}(\omega)$ of the *XX* model can be reproduced by means of the recursion method with relative ease. It is determined by the linear sequence

$$\Delta_k^{xx}(\infty)=\tfrac{1}{2}J^2k\quad(J_z=0) \tag{4.1}$$

via (2.4) and (2.5).[21] The strength of the continued-fraction analysis of this function derives from the fact that gradual deviations from the exactly solvable limit $J_z=0$ produce only gradual deviations from (4.1). The resulting nearly linear Δ_k sequences, in turn, produce gradual changes in the spectral density $\Phi_\infty^{xx}(\omega)$.

As J_z increases from zero, we can identify two types of systematic deviations of the Δ_k's from the linear sequence (4.1): (i) A gradual increase in growth rate λ implies a gradual change in the decay law at large ω of the spectral density according to the following relation:[31,32]

$$\Delta_k^{\mu\mu}(l)\sim k^\lambda \Longleftrightarrow \Phi_l^{\mu\mu}(\omega)\sim\exp(-|\omega|^{2/\lambda})\ . \tag{4.2}$$

(ii) Gradually increasing alternating deviations of the Δ_k's from the line k^λ signal the emergence of a power-law singularity at $\omega=0$ in the spectral density and allow for an estimate of the singularity exponent.[23,30] Both effects are illustrated in Fig. 2. The main plot shows $\ln\Delta_k$ versus $\ln k$ for two cases of the *XXZ* model. The open circles represent the linear sequence (4.1) for $J_z=0$, which has slope $\lambda=1$. The regression line for $J_z=J$ has slope $\lambda\simeq1.22$. The predominantly alternating deviations of the full circles from that line are clearly visible. The inset shows the variation of the growth rate λ with J_z between the *XX* and *XXX* models.[33] Changes in growth rate over that range have only negligible impact on the physically interesting structures in the spectral densities investigated here. The growing alternating deviations in the Δ_k sequence are the signature of an emerging infrared divergence implied by the spin-diffusive long-time tail that is

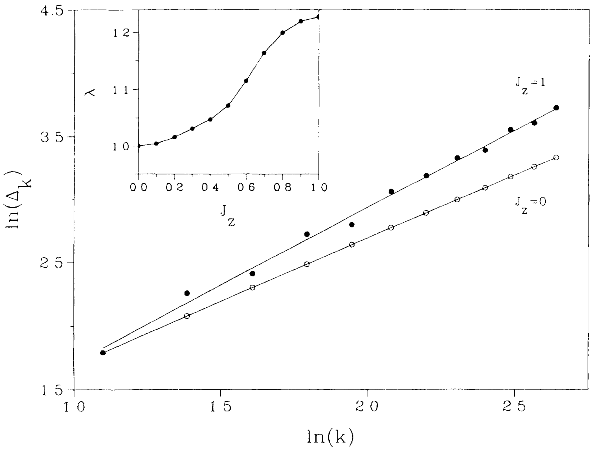

FIG. 2. Log-log plot of the sequences $\Delta_k^{xx}(\infty)$ for the bulk-spin-autocorrelation function $\langle S_\infty^x(t) S_\infty^x \rangle$ at $T=\infty$ of the 1D $s=\frac{1}{2}$ XX model ($J=1, J_z=0$) and XXX model ($J=J_z=1$). The slope of the linear regression lines determines the growth rate λ of each Δ_k sequence. The inset shows λ as a function of J_z (for $J=1$).

expected to dominate the function $\langle S_\infty^x(t) S_\infty^x \rangle$ for $J_z=J$. A quantitative analysis of that singularity will be presented in Sec. IV C. It yields strong evidence for a transition from an unconstrained relaxation process at $J_z<J$ to a diffusion process at $J_z=J$ in the fluctuations of $S_\infty^x(t)$.

For the reconstruction of spectral densities from Δ_k sequences with growth rates $\lambda \simeq 1$, we have proposed and successfully employed the following procedure:[29,30] (i) Pick a Gaussian model spectral density, $\bar{\Phi}(\omega)=(2\sqrt{\pi}/\omega_0)\exp(-\omega^2/\omega_0^2)$. (ii) Expand the associated model relaxation function (2.4) into a continued fraction down to level n; this generates the model coefficients $\bar{\Delta}_k=\omega_0^2 k/2$ and defines the nth-level termination function $\Gamma_n(z)$. (iii) Determine the parameter ω_0 by matching the slope of $\bar{\Delta}_k$ versus k with the average slope of $\Delta_k^{xx}(\infty)$ vs k for the finite sequence of coefficients $\Delta_1^{xx}(\infty), \ldots, \Delta_n^{xx}(\infty)$ pertaining to the dynamical quantity of interest and inferred from exact moments or produced by the recursion method. (iv) Replace the model coefficients $\bar{\Delta}_1, \ldots, \bar{\Delta}_n$ by the known system coefficients $\Delta_1^{xx}(\infty), \ldots, \Delta_n^{xx}(\infty)$ in the relaxation function and evaluate the spectral density via (2.5). That is the recipe for reconstructing spectral densities by means of a *Gaussian terminator.*

For Δ_k sequences whose growth rates deviate significantly from $\lambda=1$ and whose spectral densities are likely to have infrared divergences as their dominant structure we should carry out such an analysis on the basis of the more general model spectral density

$$\bar{\Phi}(\omega)=\frac{2\pi/\lambda\omega_0}{\Gamma\left[\frac{\lambda}{2}(1+\alpha)\right]}\left|\frac{\omega}{\omega_0}\right|^{\alpha}\exp(-|\omega/\omega_0|^{2/\lambda}) . \quad (4.3)$$

This remains impractical as long as we lack closed-form expressions for the model continued-fraction coefficients Δ_k pertaining to (4.3) as functions of the three parameters $\omega_0, \alpha, \lambda$. However, for growth rates sufficiently close to $\lambda=1$, we can approximate the ($\lambda \neq 1$) problem with a ($\lambda=1$) problem if we replace the Δ_k sequence by the rescaled sequence

$$\Delta_k^* = \Delta_k^{1/\lambda} \quad (4.4)$$

and then proceed as outlined previously. The main distortions in the reconstructed spectral density caused by this approximation are of two kinds: (i) a change in the large-ω decay law and (ii) a change in the frequency scale. Whereas the former effect has only a negligible impact on the shape of the spectral-weight distribution, the latter may warrant attention and lead to significant improvement upon proper adjustment.[34]

B. Reconstruction of spectral densities

We have reconstructed the bulk-spin spectral density $\Phi_\infty^{xx}(\omega)$ of the XXZ model for $0 \le J_z/J \le 1$ by using the continued-fraction coefficients $\Delta_1^{xx}(\infty), \ldots, \Delta_{14}^{xx}(\infty)$ inferred from the moments tabulated in Appendix A and a Gaussian terminator with its parameter determined from the slope of the Δ_k^* sequence.

Figure 3 shows the reconstructed function $\Phi_\infty^{xx}(\omega)$, at $\omega<0$ for values of the anisotropy parameter between $J_z/J=0$ and $J_z/J=0.5$, and at $\omega>0$ for parameter values between $J_z/J=0.6$ and $J_z/J=1.0$. The five curves on the left illustrate how the pure Gaussian (3.2) (dashed line) evolves into a curve with some structure as J_z/J increases from zero. The additional structure consists of (i) a central peak of increasing height and decreasing width and (ii) a shoulder of enhanced spectral weight

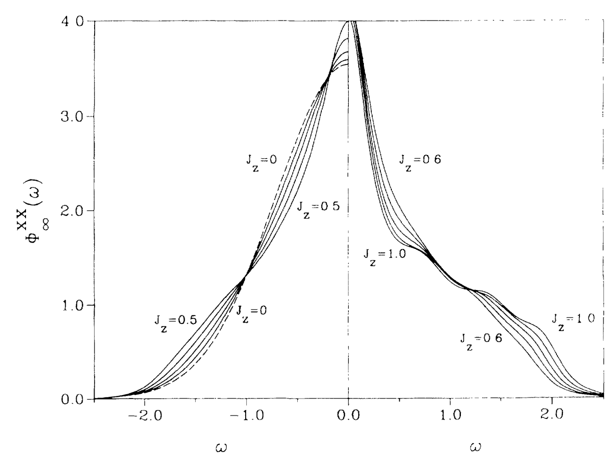

FIG. 3. Spectral density $\Phi_\infty^{xx}(\omega)$ at $T=\infty$ of the 1D $s=\frac{1}{2}$ XXZ model with $J=1$ as reconstructed from the continued-fraction coefficients $\Delta_1^{xx}(\infty), \ldots, \Delta_{14}^{xx}(\infty)$ and a Gaussian terminator. The calculation was carried out by the use of the Δ_k^* sequence in the role of the original Δ_k sequence. The four solid curves for $\omega<0$ pertain to the values $J_z=0.2, \ldots, 0.5$ of the anisotropy parameter and the five curves plotted for $\omega>0$ to values $0.6, \ldots, 1.0$. The dashed curve represents the exact result (3.2) for the case $J_z=0$. The result for $J_z=0.1$ (not shown) deviates from that for $J_z=0$ by amounts comparable to the thickness of the dashed line.

at $\omega \simeq 1.5J$. The further development of the spectral density as J_z/J approaches the XXX case is shown by the curves on the right. The shoulder becomes more pronounced, and the strong peak at $\omega=0$, signals the presence of an infrared divergence for $J_z=J$ in accordance with spin-diffusion phenomenology.

The curve for the XXX case is in qualitative agreement with previous results obtained from finite-chain calculations,[3,4] and by a calculation which uses the first two frequency moments of the dynamic structure factor in conjunction with a two-parameter diffusivity.[6] We should like to emphasize that the infrared singularity in $\Phi_\infty^{xx}(\omega)$, which is strongly suggested by the curves for $J_z/J \simeq 1$ in Fig. 3, is in no way artificially built into our approach. It is a structure resulting solely from the 14 known continued-fraction coefficients.

The reconstructed spectral density $\Phi_\infty^{xx}(\omega)$ shown in Fig. 3 is expected to be most accurate for small values of J_z/J, where the growth rate is closest to $\lambda=1$ (see Fig. 2, inset). As the growth rate increases toward $\lambda \simeq 1.22$, the curves are likely to become subject to the abovementioned systematic errors. We have estimated the systematic error in frequency scale not to exceed 2% for the curves at $0<J_z/J\leq 0.5$ and 12% for those at $0.5<J_z/J\leq 1$.

C. Analysis of infrared singularities

For a quantitative analysis of the infrared singularity in the spectral density $\Phi_\infty^{xx}(\omega)$, we focus on the alternating deviations about the average (nearly linear) growth of the Δ_k sequences. Consider the special case $\lambda=1$ of the model spectral density (4.3). The associated Δ_k sequence is known in closed form:[29]

$$\bar{\Delta}_{2k-1}=\tfrac{1}{2}\omega_0^2(2k-1+\alpha),\quad \bar{\Delta}_{2k}=\tfrac{1}{2}\omega_0^2(2k)\ . \qquad (4.5)$$

For this model spectral density, the singularity exponent α is determined by the displacement of the $\bar{\Delta}_{2k-1}$ from the line $\bar{\Delta}_{2k}=\omega_0^2 k$. In real situations, that displacement is subject to "fluctuations" caused by other structures in the spectral density. The exponent α of the infrared singularity can nevertheless be estimated from the average distance in vertical displacement of the Δ_{2k} and the Δ_{2k-1} from the linear regression line for the entire sequence. Two previous applications of that procedure yielded reasonable results.[23,30]

The results of such an analysis applied to the Δ_k^* sequences inferred from 14 exact moments are compiled in Fig. 4. The full circles joined by solid lines represent the mean exponent values α as a function of J_z/J ranging from the XX model ($J_z=0$) to the XXX model ($J_z=J$) and somewhat beyond. The error bars indicate the statistical uncertainty for each data point, which is due to the fact that the analysis is based on a finite number of known continued-fraction coefficients. On top of the statistical error, the data are likely to be subject to a systematic error whose potential impact increases with the deviation of the growth rate from $\lambda=1$. We have yet to design a simple and satisfactory way to correct for systematic errors in the exponent analysis. As J_z approaches zero, both types of uncertainties (statistical and systematic) become smaller and disappear. The data point $\alpha(0)=0$ is exact and describes the spectral density (3.2), which has no infrared singularity.

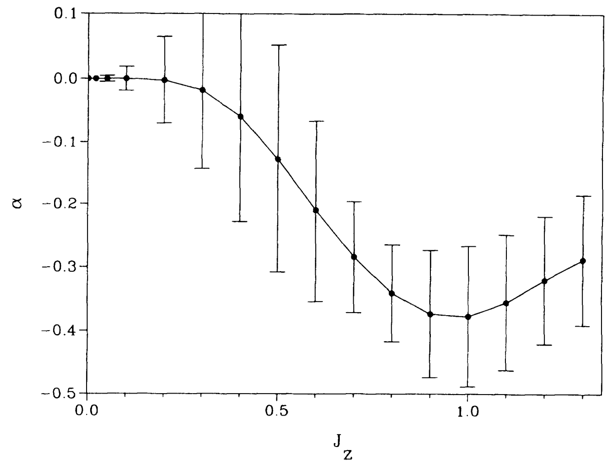

FIG. 4. Infrared-singularity exponent α versus anisotropy parameter J_z of the spectral density $\Phi_\infty^{xx}(\omega)$ at $T=\infty$ of the 1D $s=\frac{1}{2}$ XXZ model with $J=1$. The data points were obtained from the continued-fraction coefficients $\Delta_3^{xx}(\infty),\ldots,\Delta_{14}^{xx}(\infty)$ by analyzing the associated Δ_k^* sequence.

In spite of the limited overall accuracy of these results, the dependence on J_z/J of the mean exponent values displayed in Fig. 4 is quite remarkable. The data strongly indicate that the function $\alpha(J_z/J)$ stays zero over some range of the anisotropy parameter. A vanishing exponent at small but nonzero J_z/J is consistent with and thus reinforces the conclusion reached from the short-time analysis that the function $\langle S_\infty^x(t)S_\infty^x\rangle$ decays faster than a power law.

While the data point at $J_z/J=0.5$ is still consistent with $\alpha=0$, the mean α values have already a strongly decreasing trend at this point. A minimum value is reached exactly at the symmetry point ($J_z=J$) of the XXX model—the only point for which the conservation law $S_T^x=\sum_i S_i^x=$const holds, and therefore the only point for which one expects a diffusive long-time tail in $\langle S_\infty^x(t)S_\infty^x\rangle$. Upon further increase of J_z/J, the data points rise again toward $\alpha=0$ as expected.

The minimum exponent value, $\alpha=-0.37\pm 0.12$, obtained for the XXX case is only marginally consistent with the standard value, $\alpha=-\frac{1}{2}$, predicted by spin-diffusion phenomenology. That discrepancy is more likely attributable to the systematic error in our data than it is evidence for anomalous spin diffusion such as was discovered in the classical 1D XXX model.[7–13]

V. SUSTAINED POWER-LAW DECAY

The conservation law $S_T^z=\sum_i S_i^z=$const for the spin fluctuations in the z direction holds over the entire parameter range of the XXZ model. Consequently, the long-time behavior of the correlation function $\langle S_\infty^z(t)S_\infty^z\rangle$ or the low-frequency behavior of the spectral density $\Phi_\infty^{zz}(\omega)$ is expected to be much less affected by the symmetry change of H_{XXZ} at $J_z = J$ than the functions $\langle S^x_\infty(t) S^x_\infty\rangle$ and $\Phi^{XX}_\infty(\omega)$ were. The verification of sustained power-law decay at $J_z \neq J$ as a contrast to the results presented in Sec. IV will further support the case for quantum spin diffusion.

Here the kind of analysis carried out previously for the reconstruction of spectral densities (Sec. IV B) and for the estimation of singularity exponents (Sec. IV C) becomes inapplicable for $0 \leq J_z/J \leq 0.6$. The breakdown is caused by a crossover in the growth rates of the relevant sequences of continued-fraction coefficients. Figure 5 shows the Δ_k sequences plotted versus k of $\Phi^{zz}_\infty(\omega)$ for four different parameter values. Between $J_z/J = 0.6$ and $J_z/J = 1.0$, the sequence of known coefficients has a well defined growth rate somewhat in excess of $\lambda = 1$. For the XX model ($J_z = 0$), on the other hand, growth rate $\lambda = 0$ is well known to be realized.[5,23] The sequence for $J_z/J = 0.1$ has attributes of both regimes. It starts out with $\lambda = 0$ up to $k \simeq 7$ and then begins to grow with $\lambda \gtrsim 1$, thus causing a kink in Δ_k versus k. That is so throughout the range $0 < J_z/J < 0.6$. It is impossible to analyze such sequences on the basis of a unique value of λ, and, therefore, impossible to carry out the analysis described before without major modifications.[35]

The bulk-spin spectral density $\Phi^{zz}_\infty(\omega)$ for four parameter values over the range $0.7 \leq J_z/J \leq 1.0$ as reconstructed from the 14 known Δ_k's and a Gaussian terminator with its parameter from the Δ^*_k sequence is displayed in Fig. 6 (solid curves). Notice how the shape of the functions $\Phi^{zz}_\infty(\omega)$ (Fig. 6) and $\Phi^{xx}_\infty(\omega)$ (Fig. 3), which start out identically, undergo different changes as the anisotropy parameter decreases from $J_z/J = 1$. While the function $\Phi^{xx}_\infty(\omega)$ gradually transforms into a pure Gaussian (dashed line in Fig. 3), the function $\Phi^{zz}_\infty(\omega)$ is supposed to approach the exact result[17]

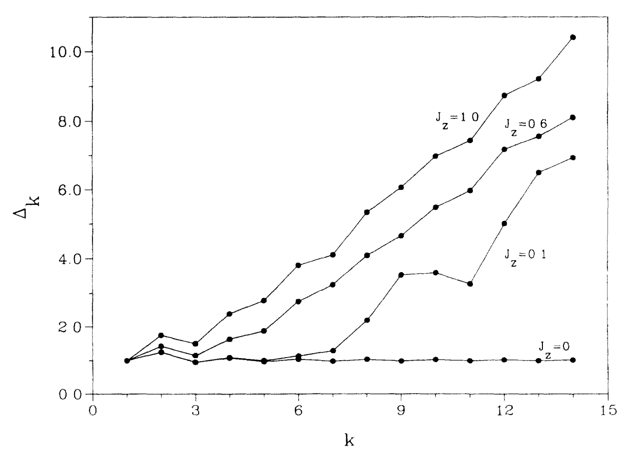

FIG. 5. Continued-fraction coefficients $\Delta^{zz}_k(\infty)$ vs k for the bulk-spin-autocorrelation function $\langle S^z_\infty(t) S^z_\infty\rangle$ at $T=\infty$ of the 1D $s=\frac{1}{2}$ XXZ model with $J=1$ and $J_z=0$ (XX case), $J_z=0.1$, 0.6, and $J_z=1.0$ (XXX case). The kink of the sequence for $J_z=0.1$ illustrates the crossover between growth rates $\lambda=0$ and $\lambda \geq 1$.

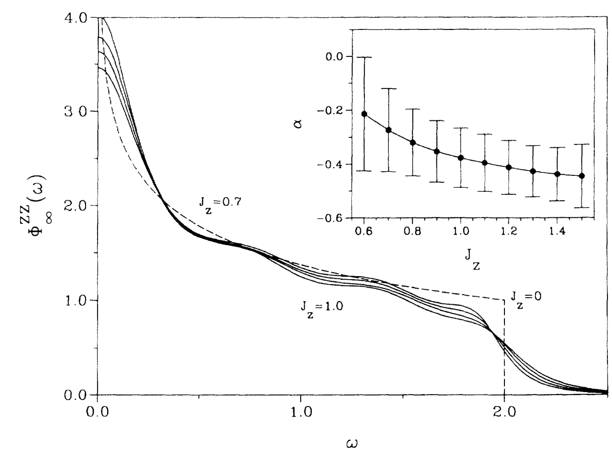

FIG. 6. Spectral density $\Phi^{zz}_\infty(\omega)$ at $T=\infty$ for the bulk-spin of the 1D $s=\frac{1}{2}$ XXZ model with $J=1$ as reconstructed from the continued-fraction coefficients $\Delta^{zz}_1(\infty), \ldots, \Delta^{zz}_{14}(\infty)$ and a Gaussian terminator. The calculation was carried out by the use of the associated Δ^*_k sequence. The four solid curves represent the cases $J_z=0.7$, 0.8, 0.9, and 1.0 (XXX model). The dashed curve is the exact result (5.1) for $J_z=0$ (XX model). In the inset we have plotted the infrared-singularity exponent α vs J_z. The data points were obtained from $\Delta^{zz}_3(\infty), \ldots, \Delta^{zz}_{14}(\infty)$ by analyzing the Δ^*_k sequence.

$$\Phi^{zz}_\infty(\omega) = \frac{2}{\pi J} K(\sqrt{1-\omega^2/4J^2})\Theta(1-\omega^2/4J^2) \quad (J_z=0) \; . \tag{5.1}$$

The graph of that complete elliptic integral has been added as dashed line to Fig. 6. The diminishing height of the central peak with decreasing J_z/J marks the weakening of the divergence from $\sim\omega^{-1/2}$ (diffusive) to $\sim\ln(1/\omega)$ (free fermions). Spectral weight removed from the central peak and from the high-frequency tail is transferred to the shoulder, which gradually transforms into a discontinuity at $\omega/J = 2$.

The inset to Fig. 6 shows our results for the infrared singularity exponent α over the parameter range $0.6 \leq J_z/J \leq 1.5$. Within the statistical uncertainties indicated by error bars, the data points are consistent with a J_z-independent exponent. This confirms that the fluctuations of S^z_l are largely unaffected by the change in the symmetry at $J_z/J = 1$ in strong contrast to our observations made in Fig. 4 for the fluctuations of S^x_l. The weak monotonic J_z dependence of the mean exponent values at $J_z/J \geq 0.8$ and their deviation from the standard value $\alpha = -0.5$ are probably attributable to the previously mentioned systematic errors, which we have not fully under control. However the sloping tendency of the mean values toward the lowest values of J_z, and the extra large error bars on those data points are an artifact caused by the crossover between growth rates as discussed in the context of Fig. 5.

VI. BOUNDARY-SPIN SPECTRAL DENSITIES

The conclusions drawn in Secs. IV and V for the bulk-spin spectral densities $\Phi^{xx}_\infty(\omega)$ and $\Phi^{zz}_\infty(\omega)$ are further substantiated when we look at the results of the same analysis carried out for the boundary-spin spectral densities $\Phi_0^{\mu\mu}(\omega)$, $\mu=x,z$. For that calculation we have 17 Δ_k's at our disposal (compared to 14 in the bulk case), but the problem with the λ crossover now plagues both x and z fluctuations for parameters $0 \le J_z/J \le 0.6$.

The spectral densities $\Phi_0^{xx}(\omega)$ for the cases $J_z/J=1.0,0.6$ as reconstructed from the Δ_k^* sequence and a Gaussian terminator are shown in Fig. 7 (solid lines). The curve for the XXX case ($J_z=J$) shows a pronounced peak at $\omega=0$. That conspicuous enhancement of spectral weight has all but disappeared for $J_z/J=0.6$, i.e., in the presence of anisotropy, where S_T^x is not conserved. Hence the central peak in the XXX result can again be interpreted as a spin-diffusive divergence.

As the anisotropy parameter is decreased below the value $J_z/J=0.6$, the shape of the function $\Phi_0^{xx}(\omega)$ must approach that of the dashed line, which represents the exact result for $J_z/J=0$,[22,23]

$$\Phi_0^{xx}(\omega)=(4/J)\sqrt{1-\omega^2/J^2} \quad (J_z=0)\ , \tag{6.1}$$

which is the Fourier transform of $\langle S_0^x(t)S_0^x\rangle=[J_0(Jt)+J_2(Jt)]/4$. While the Δ_k^* analysis breaks down for small values of J_z/J, the way the function $\Phi_0^{xx}(\omega)$ develops between $J_z/J=1.0$ and 0.6 can be extrapolated fairly smoothly toward the dashed line.

We have calculated the infrared-singularity exponent α of the boundary-spin spectral density $\Phi_0^{xx}(\omega)$ over the extended parameter range $0.6 \le J_z/J \le 1.2$ by means of the analysis explained previously. The inset to Fig. 7 shows seven equally spaced data points on that interval. The α values at the endpoints of the interval are very close to zero. In between, the data points drop toward a minimum, again located at the symmetry point $J_z=J$, where the conservation law $S_T^x=$const holds. The exponent value at the minimum, $\alpha=-0.45\pm0.26$, is consistent with spin-diffusion phenomenology.

Note the strongly contrasting J_z dependence of the singularity exponent pertaining to the spectral density $\Phi_0^{zz}(\omega)$ as shown in the inset to Fig. 8. Here the data points indicate the presence of an infrared divergence over the entire parameter range shown. However, a much stronger J_z dependence of the mean values of α is indicated than was the case of the corresponding bulk-spin results (Fig. 6). Whether that J_z dependence is entirely attributable to the systematic errors in our analysis and to the λ crossover remains to be seen.

In view of the fact that infrared divergences are likely to be real in the function $\Phi_0^{zz}(\omega)$ for all values of $J_z>0$, we have treated them as such for its reconstruction from the known Δ_k's. Instead of using a Gaussian terminator (cf. Sec. IV A), which is completely unbiased with respect to the spectral-weight distribution at low frequencies, we have used a two-parameter terminator with built-in infrared divergence. Its model relaxation function has been determined numerically via

$$\bar{c}(z)=\frac{1}{2\pi i}\int_{-\infty}^{+\infty} d\omega \frac{\bar{\Phi}(\omega)}{\omega-iz} \tag{6.2}$$

from the model spectral density (4.3) with $\lambda=1$. The value of the parameter ω_0 is determined by the slope of Δ_k versus k as before and the parameter α by our estimate of the singularity exponent.

Two of the curves in the main plot of Fig. 8 represent

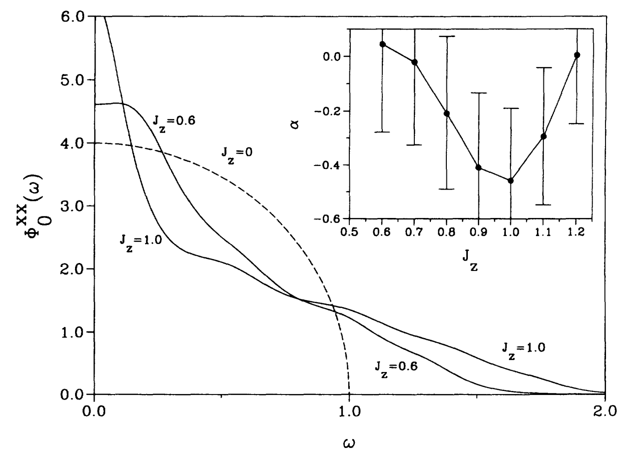

FIG. 7. Spectral density $\Phi_0^{xx}(\omega)$ at $T=\infty$ for the boundary spin of the semi-infinite 1D $s=\frac{1}{2}$ XXZ model with $J=1$ as reconstructed from the continued-fraction coefficients $\Delta_1^{xx}(0),\ldots,\Delta_{17}^{xx}(0)$ and a Gaussian terminator. The calculation was carried out with the associated Δ_k^* sequence. The two solid curves represent the cases $J_z=1.0$ (XXX model) and $J_z=0.6$. The dashed curve is the exact result (6.1) for $J_z=0$ (XX model). In the inset we have plotted the infrared-singularity exponent α vs J_z. The data points were obtained from $\Delta_5^{xx}(0),\ldots,\Delta_{17}^{xx}(0)$ by analyzing the Δ_k^* sequence.

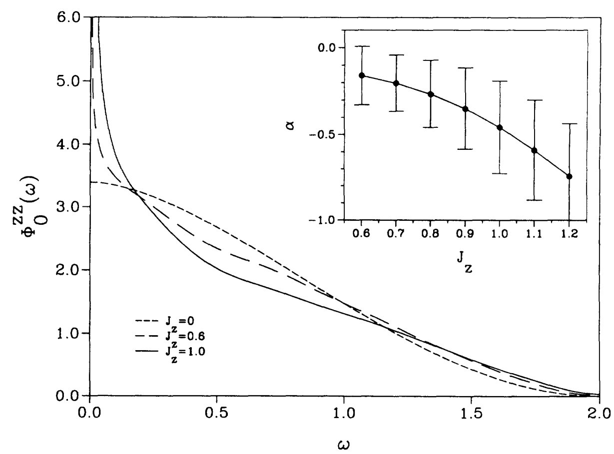

FIG. 8. Spectral density $\Phi_0^{zz}(\omega)$ at $T=\infty$ for the boundary-spin of the semi-infinite 1D $s=\frac{1}{2}$ XXZ model with $J=1$ as reconstructed from the continued-fraction coefficients $\Delta_1^{zz}(0),\ldots,\Delta_{17}^{zz}(0)$ and a special terminator with built-in infrared divergence. The calculation was carried out with the associated Δ_k^* sequence for the two cases $J_z=1.0$ (XXX model) and $J_z=0.6$. Also shown is the exact result (6.3) for $J_z=0$ (XX model). In the inset we have plotted the infrared-singularity exponent α vs J_z. The data points were obtained from $\Delta_5^{zz}(0),\ldots,\Delta_{17}^{zz}(0)$ by analyzing the Δ_k^* sequence.

TABLE I. Coefficients $m_{2k}^{zz}(\infty, 2n)$ of the expansion (A1).

(a)

n \ k	0	1	2	3	4	5	6	7	8	9	10
0	1	4	36	400	4900	63 504	853 776	11 778 624	165 636 900	2 363 904 400	34 134 779 536
1			8	220	4928	102 816	2 082 432	41 889 276	853 435 440	18 007 681 120	404 357 922 176
2				32	1680	65 040	2 202 552	69 951 024	2 185 202 448	70 013 058 128	2 392 462 416 032
3					128	10 944	690 624	36 246 496	1 698 825 024	75 435 121 632	3 333 426 429 472
4						512	64 768	6 755 840	549 482 752	37 407 224 320	2 310 521 698 496
5							2 048	359 424	68 143 104	8 681 526 272	845 021 416 448
6								8 192	1 904 640	773 124 096	149 994 047 488
7									32 768	9 748 480	10 104 356 864
8										131 072	48 562 176
9											524 288

(b)

n \ k	11	12	13	14
0	497 634 306 624	7 312 459 672 336	108 172 480 360 000	1 609 341 595 560 000
1	9 949 668 294 384	274 306 374 598 816	8 515 165 277 366 400	293 689 049 445 227 520
2	90 108 145 903 328	3 818 389 970 787 536	183 158 941 471 799 360	9 897 648 485 066 180 280
3	152 518 390 778 192	7 437 658 317 638 080	393 511 098 121 688 320	22 788 275 253 904 140 480
4	137 597 279 684 160	8 235 302 175 513 088	508 357 918 320 849 920	32 861 130 914 036 446 560
5	71 399 519 201 920	5 659 100 274 909 696	439 582 513 633 988 480	34 262 961 004 473 446 400
6	20 036 827 439 104	2 241 971 015 355 904	230 682 233 804 249 600	22 813 769 083 856 071 680
7	2 777 636 151 296	483 625 025 896 448	69 194 244 489 041 920	9 011 556 663 726 581 760
8	146 673 500 160	53 025 275 772 928	11 535 327 478 087 680	2 057 482 151 063 347 200
9	236 716 032	2 253 105 659 904	1 016 515 896 279 040	268 256 018 812 108 800
10	2 097 152	1 133 510 656	35 490 737 684 480	19 343 088 683 581 440
11		8 388 608	5 347 737 600	564 637 653 270 528
12			33 554 432	24 914 165 760
13				134 217 728

TABLE II. Coefficients $m_{2k}^{xx}(\infty,2n)$ of the expansion (A1).

(a)

n \ k	0	1	2	3	4	5	6	7	8	9	10
0	1	2	12	120	1680	30 240	665 280	17 297 280	518 918 400	17 643 225 600	670 442 572 800
1		2	24	260	3024	40 320	680 064	16 024 008	511 299 360	19 380 359 856	790 533 972 800
2			8	240	5012	96 480	1 863 576	38 116 936	904 349 732	28 564 911 232	1 254 507 751 744
3				32	1792	63 744	1 953 776	56 926 012	1 645 089 888	49 127 454 896	1 650 071 143 616
4					128	11 520	663 872	31 787 392	1 384 501 248	57 265 586 368	2 314 444 556 752
5						512	67 584	6 456 320	490 989 056	31 918 392 704	1 884 787 750 016
6							2 048	372 736	65 516 544	8 028 291 072	762 099 244 032
7								8 192	1 966 080	753 139 712	143 168 688 128
8									32 768	10 027 008	9 966 141 440
9										131 072	49 807 360
10											524 288

(b)

n \ k	11	12	13	14
0	28 158 588 057 600	1 295 295 050 649 600	64 764 752 532 480 000	3 497 296 636 753 920 000
1	33 192 199 504 464	1 410 744 469 720 768	60 363 991 751 481 600	2 604 924 609 998 538 240
2	67 752 201 558 496	3 955 582 832 037 408	234 928 426 159 350 720	13 894 163 289 895 006 800
3	71 440 014 187 376	4 224 665 438 128 064	306 448 398 158 942 240	24 028 691 547 335 252 400
4	94 831 675 835 968	4 249 623 524 974 624	235 784 156 426 515 200	17 376 963 387 911 026 200
5	105 259 016 639 040	5 715 363 282 918 656	310 980 152 826 272 160	17 917 127 977 298 169 600
6	62 721 972 915 712	4 772 749 197 832 832	347 319 490 135 290 880	24 683 103 277 934 568 960
7	18 825 129 374 720	2 069 331 679 262 720	207 177 188 266 183 680	19 623 106 832 018 688 000
8	2 705 189 994 496	465 152 129 253 376	65 657 336 480 194 560	8 385 642 509 287 802 880
9	145 781 686 272	52 188 717 776 896	11 232 579 986 063 360	1 982 528 585 053 962 240
10	242 221 056	2 247 649 132 544	1 005 690 153 861 120	262 983 884 215 418 880
11	2 097 152	1 157 627 904	35 458 729 902 080	19 188 697 927 778 304
12		8 388 608	5 452 595 200	564 456 232 845 312
13			33 554 432	25 367 150 592
14				134 217 728

TABLE III. Coefficients $m_{2k}^{zz}(0,2n)$ of the expansion (A1).

(a)

n \ k	0	1	2	3	4	5	6	7	8	9	10	11	12
0	1	2	10	70	588	5544	56 628	613 470	6 952 660	81 662 152	987 369 656	12 228 193 432	154 532 114 800
1			2	28	360	4752	65 494	940 940	14 014 936	215 358 312	3 404 469 096	55 363 106 984	929 065 985 440
2				2	54	1166	24 310	515 866	11 203 816	247 345 648	5 523 685 016	124 847 197 736	2 872 036 690 580
3					2	88	3 172	107 848	3 651 328	121 432 496	3 906 907 224	121 505 574 104	3 685 085 980 110
4						2	130	8 422	476 952	25 617 776	1 263 625 096	56 622 505 150	2 337 161 324 250
5							2	180	24 208	2 201 568	181 559 326	12 792 785 196	769 533 217 540
6								2	238	78 622	10 508 178	1 301 095 050	127 543 927 220
7									2	304	282 764	50 716 840	9 484 170 520
8										2	378	1 079 574	243 836 340
9											2	460	4 239 160
10												2	550
11													2
12													

(b)

n \ k	13	14	15	16	17
0	1 986 841 476 000	25 928 281 261 800	342 787 130 211 150	4 583 937 702 039 300	61 923 368 957 373 000
1	16 200 874 954 800	296 826 867 484 110	5 798 385 460 938 540	122 683 556 698 067 640	2 845 789 468 891 344 360
2	67 890 211 103 550	1 669 240 405 921 410	43 248 167 869 956 330	1 194 139 339 025 630 880	35 384 641 175 890 921 200
3	110 439 371 747 760	3 319 961 677 623 180	101 660 119 675 188 840	3 216 997 000 723 115 040	106 463 055 861 804 168 000
4	90 795 109 218 210	3 393 450 440 061 390	124 563 577 907 601 990	4 577 021 767 825 432 560	171 239 371 535 145 995 280
5	40 826 968 637 160	1 977 777 380 312 910	90 156 050 230 686 660	3 968 230 388 536 813 920	172 476 952 938 667 790 880
6	10 024 095 487 800	667 749 304 798 500	39 568 059 743 658 690	2 166 081 794 234 685 000	112 937 338 652 691 902 880
7	1 267 861 285 560	127 114 676 648 580	10 415 737 182 535 680	742 482 232 802 603 520	48 167 235 794 519 032 848
8	71 037 833 760	12 668 494 432 980	1 582 205 326 125 582	156 452 354 927 034 600	13 216 836 286 918 095 200
9	1 160 354 160	551 174 008 758	127 569 295 601 676	19 392 025 540 363 632	2 274 442 513 310 739 376
10	16 840 110	5 457 004 878	4 439 474 838 250	1 292 809 502 109 968	234 196 749 152 251 744
11	648	67 194 740	25 374 030 472	36 982 403 631 424	13 144 773 384 271 072
12	2	754	268 550 086	116 779 829 680	316 381 035 096 352
13		2	868	1 073 891 872	532 591 267 008
14			2	990	4 295 160 382
15				2	1 120
16					2

TABLE IV. Coefficients $m_{2k}^{xx}(0,2n)$ of the expansion (A1).

(a)

n \ k	0	1	2	3	4	5	6	7	8	9	10	11	12
0	1	1	2	5	14	42	132	429	1 430	4 862	16 796	58 786	208 012
1		1	9	57	350	2388	20 097	218 361	2 962 674	47 080 956	833 526 694	15 951 526 836	324 134 817 864
2			1	37	500	5085	47 817	473 473	5 575 596	85 693 634	1 722 480 188	41 925 608 012	1 140 770 228 156
3				1	139	3505	57 442	801 801	10 914 852	158 009 560	2 578 845 566	49 632 904 812	1 166 216 432 693
4					1	531	22 170	554 125	11 402 016	224 117 120	4 527 076 268	96 018 517 173	2 130 778 265 785
5						1	2 077	130 305	4 711 604	138 323 696	3 836 625 331	107 115 195 473	3 044 719 656 316
6							1	8 233	723 144	36 498 371	1 493 932 969	57 083 748 637	2 141 724 513 162
7								1	32 823	3 837 537	265 712 036	15 015 598 665	777 193 603 198
8									1	131 143	19 666 510	1 868 948 535	145 643 240 124
9										1	524 377	98 050 337	13 023 969 650
10											1	2 097 261	478 162 812
11												1	8 388 739
12													1

(b)

n \ k	13	14	15	16	17
0	742 900	2 674 440	9 694 845	35 357 670	129 644 790
1	6 913 406 747 380	153 528 931 055 925	3 528 532 718 636 985	83 533 373 812 739 370	2 029 335 527 879 237 820
2	33 042 919 449 445	994 756 201 541 865	30 804 691 063 777 785	977 819 691 333 030 060	31 820 503 528 097 882 070
3	33 468 632 359 985	1 120 172 089 579 650	41 108 492 444 365 065	1 580 601 989 312 755 560	62 156 677 031 439 043 440
4	49 438 484 953 055	1 226 557 118 119 230	34 286 322 185 445 825	1 140 778 568 680 224 000	45 259 587 069 153 790 680
5	87 280 993 610 105	2 496 266 577 874 515	70 936 357 456 591 545	2 018 054 068 801 574 280	59 106 036 083 022 711 960
6	79 551 764 550 480	2 913 957 297 036 015	104 895 736 359 160 905	3 709 454 596 717 102 080	129 278 403 677 771 856 300
7	38 257 727 114 940	1 810 145 263 080 690	82 730 076 297 083 385	3 670 990 174 588 316 700	159 085 198 123 172 037 048
8	10 055 495 062 500	635 171 773 479 930	37 449 331 649 060 445	2 093 100 135 486 779 760	112 327 113 474 260 368 824
9	1 399 825 120 580	126 488 156 851 605	10 025 102 368 543 713	722 421 733 226 903 820	48 591 706 611 682 667 464
10	91 975 566 665	13 549 528 822 377	1 564 366 561 926 945	152 179 442 064 682 488	13 181 808 438 206 934 780
11	2 290 106 897	670 347 869 790	132 967 383 212 721	19 097 204 936 013 832	2 235 049 510 341 476 016
12	33 554 587	10 804 550 050	5 097 573 875 065	1 322 567 599 253 088	230 208 596 780 129 760
13	1	134 217 909	50 331 678 465	40 527 104 759 752	13 282 222 997 574 528
14		1	536 871 121	231 928 273 680	335 075 020 631 015
15			1	2 147 483 887	1 058 709 489 345
16				1	8 589 934 863
17					1

the function $\Phi_0^{zz}(\omega)$ for $J_z/J=1.0$ and $J_z/J=0.6$ as reconstructed form the 17 known continued-fraction coefficients and this special terminator. As the parameter drops from the higher to the lower value, the central peak in the spectral density weakens considerably, and the weak shoulder at $\omega=J$ present for $J_z/J=1.0$ all but disappears. Upon further decrease of J_z/J to zero (*XX* model), the curve is supposed to approach the dashed line, which is the known exact result[23]

$$\Phi_0^{zz}(\omega)=\frac{128}{3\pi J}(1+\omega/2J)\left[(1+\omega^2/4J^2)E\left[\frac{2J-\omega}{2J+\omega}\right]-\frac{\omega}{J}K\left[\frac{2J-\omega}{2J+\omega}\right]\right]. \tag{6.3}$$

This limiting case is perfectly in line with how the reconstructed spectral density develops between $J_z/J=1.0$ and $J_z/J=0.6$.

ACKNOWLEDGMENTS

The work done at URI was supported by the U.S. National Science Foundation, Grants No. DMR-90-07540 and DMR-93-12252. Access to supercomputers at the National Center for Supercomputing Applications, University of Illinois Urbana-Champaign, is gratefully acknowledged. J.S. gratefully acknowledges support by the Max Kade Foundation. M.B. wishes to thank Hajo Leschke for helpful discussions and the Studienstiftung des deutschen Volkes for support.

APPENDIX A

The frequency moments (2.2) of the spectral density (1.3) as expressed in terms of the expectation values (2.3) yield upon evaluation, for the *XXZ* model (1.1), expressions of the form

$$M_{2k}^{\mu\mu}(l)=2^{-2k}\sum_{n=0}^{k} m_{2k}^{\mu\mu}(l,2n)J_z^{2n}J^{(2k-2n)} \tag{A1}$$

with integer coefficients $m_{2k}^{\mu\mu}(l,2n)$. We have computed these coefficients up to $k=14$ for the bulk spin ($l=\infty$) and up to $k=17$ for the boundary spin ($l=0$). The former are listed in Table I for $\mu=z$ and Table II for $\mu=x$, the latter in Table III for $\mu=z$ and Table IV for $\mu=x$.

APPENDIX B

The first K expansion coefficients M_{2k}, $k=1,\ldots,K$ of an autocorrelation function (1.2) (or frequency moments of its Fourier transform) determine the first K continued-fraction coefficients Δ_k, $k=1,\ldots,K$ of its Laplace transform (2.4) and vice versa. The Δ_k, for example, are expressible in terms of Hankel determinants with elements consisting of moments M_{2k}.[5,36,37] There exist several different algorithms for the numerical conversion of one set of numbers into the other. Some of them are more susceptible to numerical instabilities than others.[37] The following algorithm,[38] which is a product of the recursion method, has proven to be fairly robust against numerical instabilities in our applications:

Forward direction: For a given set of moments M_{2k}, $k=0,1,\ldots,K$ with $M_0=1$, the first K coefficients Δ_m, are determined by

$$M_{2k}^{(m)}=\frac{M_{2k}^{(m-1)}}{\Delta_{m-1}}-\frac{M_{2k-2}^{(m-2)}}{\Delta_{m-2}},\quad \Delta_m=M_{2m}^{(m)} \tag{B1}$$

for $k=m,m+1,\ldots,K$ and $m=1,2,\ldots,K$ and with set values $M_{2k}^{(0)}=M_{2k}$, $\Delta_{-1}=\Delta_0=1$, $M_{2k}^{(-1)}=0$.

Reverse direction: For a given set of $\Delta_m=M_{2m}^{(m)}$, $m=1,\ldots,K$, and $\Delta_{-1}=\Delta_0=1$, the moments $M_{2n}^{(0)}=M_{2n}$, result from the relations,

$$M_{2k}^{(m-1)}=\Delta_{m-1}M_{2k}^{(m)}+\frac{\Delta_{m-1}}{\Delta_{m-2}}M_{2k-2}^{(m-2)} \tag{B2}$$

for $m=k,k-1,\ldots,1$ and $k=1,2,\ldots,K$ and with set values $M_{2k}^{(-1)}=0$.

---

*On leave from Institut für Physik, Universität Dortmund, D-44221 Dortmund, Germany. Present address: Lehrstuhl für Theoretische Physik I, Universität Bayreuth D-95440 Bayreuth, Germany.

[1]D. Hone, C. Scherer, and F. Borsa, Phys. Rev. B **9**, 965 (1974); F. Borsa and M. Mali, *ibid.* **9**, 2215 (1974); J.-P. Boucher, M. Ahmed Bakheit, M. Nechtshein, M. Villa, G. Bonera, and F. Borsa, *ibid.* **13**, 4098 (1976).
[2]A. Lagendijk and E. Siegel, Solid State Commun. **20**, 709 (1976).
[3]F. Carboni and P. M. Richards, Phys. Rev. **177**, 889 (1969).
[4]J. P. Groen, T. O. Klaassen, N. J. Poulis, G. Müller, H. Thomas, and H. Beck, Phys. Rev. B **22**, 5369 (1980).
[5]J. M. R. Roldan, B. M. McCoy, and J. H. H. Perk, Physica A **136**, 255 (1986).
[6]R. A. Tahir-Kheli and D. G. McFadden, Phys. Rev. **178**, 800 (1969).
[7]G. Müller, Phys. Rev. Lett. **60**, 2785 (1988).
[8]R. W. Gerling and D. P. Landau, Phys. Rev. Lett. **63**, 812 (1989).
[9]G. Müller, Phys. Rev. Lett. **63**, 813 (1989).
[10]R. W. Gerling and D. P. Landau, Phys. Rev. B **42**, 8214 (1990).
[11]J.-M. Liu, N. Srivastava, V. S. Viswanath, and G. Müller, J. Appl. Phys. **70**, 6181 (1991).
[12]O. F. De Alcantara Bonfim and G. Reiter, Phys. Rev. Lett. **69**, 367 (1992).
[13]M. Böhm, R. W. Gerling, and H. Leschke, Phys. Rev. Lett. **70**, 248 (1993).
[14]M. H. Lee, I. M. Kim, and R. Dekeyser, Phys. Rev. Lett. **52**, 1579 (1984); R. Dekeyser and M. H. Lee, Phys. Rev. B **43**, 8123, 8131 (1991).
[15]J.-M. Liu and G. Müller, Phys. Rev. A **42**, 5854 (1990).
[16]Th. Niemeijer, Physica **36**, 377 (1967).

[17]S. Katsura, T. Horiguchi, and M. Suzuki, Physica **46**, 67 (1970).

[18]A. Sur, D. Jasnow, and I. J. Lowe, Phys. Rev. B **12**, 3845 (1975).

[19]U. Brandt and K. Jacoby, Z. Phys. B **25**, 181 (1976).

[20]H. W. Capel and J. H. H. Perk, Physica **87A**, 211 (1977); J. H. H. Perk and H. W. Capel, *ibid.* **89A**, 265 (1977).

[21]J. Florencio and M. H. Lee, Phys. Rev. B **35**, 1835 (1987).

[22]S. Sen, Phys. Rev. B **44**, 7444 (1991).

[23]J. Stolze, V. S. Viswanath, and G. Müller, Z. Phys. B **89**, 45 (1992).

[24]U. Brandt and J. Stolze, Z. Phys. B **64**, 327 (1986).

[25]M. Böhm and H. Leschke, J. Phys. A **25**, 1043 (1992).

[26]M. Böhm and H. Leschke, Physica A **199**, 116 (1993); **203**, 328 (1994).

[27]O. Platz and R. G. Gordon, Phys. Rev. Lett. **30**, 264 (1973); Phys. Rev. B **7**, 4764 (1973).

[28]M. H. Lee, Phys. Rev. Lett. **49**, 1072 (1982); Phys. Rev. B **26**, 2547 (1982).

[29]V. S. Viswanath and G. Müller, J. Appl. Phys. **67**, 5486 (1990).

[30]V. S. Viswanath and G. Müller, J. Appl. Phys. **70**, 6178 (1991).

[31]A. Magnus, in *The Recursion Method and Its Applications,* edited by D. G. Pettifor and D. L. Weaire (Springer-Verlag, New York, 1985), p. 22.

[32]D. S. Lubinsky, Acta Appl. Math. **10**, 237 (1987).

[33]What looks like a gradual increase of λ may, in fact be a crossover between two fixed values of growth rate, one for free fermions ($\lambda=0$) and another one for interacting fermions ($\lambda\simeq 1.2$). What counts for our analysis is the effective growth rate pertaining to the known finite Δ_k sequence.

[34]It is no problem to design adjustments that remove some of the most obvious systematic errors in the results presented in Secs. IV–VI and to justify these corrections by very reasonable arguments. However, there is some ambiguity in how to implement these adjustments. This makes it hard to fully detach the choice of implementation from hindsight knowledge. We have decided, therefore, to present our results here without any such adjustments for systematic errors.

[35]If the kink occurs at sufficiently large values of k, one might be tempted to analyze that Δ_k sequence on the basis of $\lambda=0$. The problem is that the interesting physics, caused by the effects of the fermion interaction for the case at hand, is contained in the Δ_k past the kink. Therefore, not much may be gained by such an exercise.

[36]M. Dupuis, Prog. Theor. Phys. **37**, 502 (1967).

[37]R. G. Gordon, J. Math. Phys. **9**, 655 (1968).

[38]V. S. Viswanath and G. Müller, *Recursion Method—Applications to Many-Body Dynamics,* Lecture Notes in Physics, Vol. m23 [Springer-Verlag, New York, in press)].